# Tuned Rib Fracture Risk Functions for Human Body Models in Frontal and Side Impacts

Jaehyuk Heo, Bronislaw Gepner, Zhaonan Sun, Jason Hallman, Jason Forman

***Abstract*** Probabilistic injury risk functions (IRFs) for human body models (HBMs) have been proposed for several body regions, including rib fracture in the thorax. Yet previous rib fracture IRFs have been tuned primarily using frontal impact data, leaving their application to lateral loading uncertain. This study extends a previously developed matched-pair tuning methodology for the thorax to side impact and evaluates whether direction-specific IRFs are required for this region. Published post-mortem human subject (PMHS) thoracic impact tests were reviewed to identify lateral cases suitable for simulation. Test-specific simulations were performed using THUMS v4.1 and GHBMC v6.0, matching impactor velocity and location while scaling impactor mass to preserve relative momentum between the impactor and subject. Maximum tensile principal strain at the 95th percentile (MPS95) from cortical rib elements was used to tune local Weibull-based IRFs via negative log-likelihood minimisation. Direction-specific IRFs derived separately from frontal and lateral datasets were similar, differing by approximately 0.25% strain at 50% predicted fracture risk. Further, combined-direction IRFs provided comparable performance and reasonably discriminated injury risk in independent whole-body sled tests. These findings suggest that HBM-specific, strain-based IRFs can be applied across frontal and lateral impact conditions within the bounds of the available PMHS data.

***Keywords*** Finite element human body models, Injury risk function, Rib fracture, Side impact, Virtual safety assessment.

## I. INTRODUCTION

Virtual crash safety assessment has the potential to complement physical testing by informing a wider range of collision and occupant conditions that may not be easily tested. Recognising this, organisations such as Euro NCAP in Europe and the Insurance Institute for Highway Safety (IIHS) in North America have been developing frameworks to incorporate virtual assessment into their evaluation programs. While their opening phases are focused on virtual assessment with dummy models, their eventual goal is to transition to human body models (HBMs) that have the potential for enhanced biofidelity and versatility beyond current dummies. Those programs anticipate providing flexibility in the choice of HBM, so long as the HBM meets certain minimum certification requirements. While those certification requirements may ensure common kinetic and kinematic biofidelity between HBMs, HBMs can also vary widely in their injury prediction. Given differences in model construction, material formulation, and output capabilities, two models can exhibit similar external biofidelity (i.e., kinetic and kinematic interaction with the surrounding environment) but very different local internal measures [1-3]. As a result, if we apply one standardised means to predict injury risk based on local internal measures, two models could predict very different injury risk even if they exhibit similar external biofidelity. Thus, the field could require that all HBMs also exhibit identical internal biofidelity and output measures (forcing such commonality as to negate the concept of model choice). Alternatively, we may accept the differences between HBMs and instead tune injury risk functions (IRFs) for each HBM to arrive at common injury risk prediction (even for models with different output measures). This type of model-specific IRF tuning method has been applied previously to rib fracture prediction [1] and pelvis fracture [4].

J. Forman (e-mail: jlf3m@virginia.edu; tel: +1-434-297-8051) is an Associate Professor and B. Gepner is a Research Associate Professor at the University of Virginia Department of Mechanical and Aerospace Engineering J. Heo is a PhD student at the University of Virginia Center for Applied Biomechanics. Z. Sun is a Principal Scientist and J. Hallman is a Senior Manager at Toyota Motor North America.

In a previous study, we developed a method to tune local, HBM-specific, strain-based thoracic injury risk functions for rib fractures in frontal impact [1]. That method involves subjecting the target HBM to a battery of 170 simulations across 13 impactor and table-top loading conditions, with each simulation representing a specific past test with a post-mortem human subject (PMHS). The outputs from the model are then combined with the injury outcomes from the PMHS tests to fit the IRF (including PMHS age as a covariate). The process was applied to the THUMS v.4.1 and GHBMC v.6.0 50th percentile males.

While directionally dependent IRFs have been the norm for physical dummies, HBMs provide the potential for universally applicable injury prediction methods that may be used across different loading modes and directions. The current study sought to expand upon our previous work, extending the strain-based IRF tuning methodology to side impact. This was accomplished by first gathering a catalogue of side-impact load cases from available literature and simulation set-up repositories. The local strain IRF tuning methodology of [1] was then applied to both the new side-impact load cases and the previous frontal-impact load cases to see if one unified IRF could be used for both.

## II. METHODS

The methods of this study followed the same general HBM-specific, IRF tuning methodology as laid out by [1] and [4], extending it to side impact of the thorax (with the THUMS v.4.1 and GHBMC v.6.0 50th percentile male HBMs). First, the literature was examined to identify prior PMHS tests involving side impact or oblique impact to the thorax, seeking studies with sufficient information to model each PMHS test. Simulation set-ups of those load cases were then gathered or built, basic biofidelity of the HBMs was checked, and the set-ups were modified so that a unique simulation was performed for each PMHS test (detailed below). Then, the probabilistic rib fracture framework of [5] was applied to predict the risk of three or more fractured ribs in each PMHS test (calculated with consideration of the age of the PMHS). The underlying local strain IRF was then tuned for each HBM using an optimisation routine minimising the sum negative log-likelihood across all simulations. The predictive ability was then validated against whole-body sled tests that were not used in the optimisation. This process was performed for the side impact cases alone, the frontal impact cases alone (refitting the frontal impact IRFs originally developed by [1] to ensure harmonisation of the methods), and for the combined dataset of the frontal and side cases.

### *Selection of Load Cases (PMHS Data)*

The literature was surveyed to identify existing side-impact PMHS studies on the thorax that could be used to develop model-specific IRFs. Since the 1970s, substantial research has informed the response and injury tolerance of the human thorax under different types of loading. This study followed the same general selection criteria used for the frontal loading conditions of [1]. This included: (1) the reference paper must include information on age, mass, and number of rib fractures for each PMHS; (2) sufficient information must be available to model the test set-ups with reasonable confidence; (3) sufficient information must be available to model the individual conditions of each test (e.g. impactor velocity). Table I gives the details of the selected load cases. The selected dataset consisted of a wide variety of loading conditions and a balance of injurious and non-injurious tests. A total of 10 impactor-type cases and five sled-type validation cases were selected. Basic illustrations of each set-up are included in Appendix A. The PMHS details and injury information for each individual test are given in Appendix A, Table A1.

TABLE I
SIDE IMPACT PMHS TEST SERIES SELECTED FOR SIMULATION

| *Type* | *PMHS Test Series* | *Loading Condition* | *No. of PMHS* | *Total no. of tests* | *No. of tests with 3+ rib fractures* | *Source of Simulation Model* |
|---|---|---|---|---|---|---|
| Impactor | Viano 1989 [6] | Rigid hub – oblique, chest | 14 | 16 | 11 | Kroell case from Toyota validation set (AM50 V4.1), modified to replicate specific load cases (impactor type or impactor location was adjusted) |
| | Viano 1989 [6] | Rigid hub – oblique, upper abdomen | | 14 | 5 | |
| | Subit 2010 [7] | Rigid bar – lateral and oblique | 3 | 13 | 3 | |
| | Shaw 2006 [8] | Rigid hub – lateral and oblique | 7 | 14 | 2 | |
| | Robbins 1979 [9] | Rigid hub – lateral | 6 | 6 | 3 | |
| | Trosseille 2008 [10] | Rigid hub – lateral and oblique | 2 | 2 | 2 | |
| | Leport 2011 [11] | Rigid hub – lateral and oblique | 8 | 8 | 8 | |
| | Kemper 2008 [12] | Rigid plate – lateral and oblique | 4 | 4 | 0 | |
| | Chung 1999 [13] | Rigid hub and rigid hub with padding – lateral and oblique | 6 | 6 | 6 | |
| | Compigne 2004 [14] | Rigid hub – lateral and oblique | 5 | 5 | 4 | |
| Sled | Petit 2019 [15] | 3-point standard belt, far side impact | 6 | 6 | 4 | Open VT |
| | Lessley 2010 [16] | Right-side pure lateral impact | 3 | 3 | 1 | [17-18] |
| | Shaw 2014 [19] | Right-side pure lateral impact with airbag | 3 | 3 | 1 | |
| | Maltese 2002 [20] | Sidewall impact with varied surface conditions | 25 | 25 | 23 | Toyota Validation Set (AM50 V4.1) |
| | Cavanaugh 1993 [21] | Sidewall impact with varied surface conditions | 17 | 17 | 15 | Toyota Validation Set (AM50 V4.1) |

***Simulation Strategy***

Before setting up the selected load cases, the HBMs were instrumented to output strains on each rib. These outputs were evaluated and utilised for the development of IRFs. The HBMs output the strains of cortical bone parts of all ribs, since the cortical shell carries most of the structural load, whereas trabecular bone is more compliant and bears less of the load. The maximum values of the maximum principal strain (MPS) time-histories sampled at 1 ms were stored for each of the individual ribs.

Simulation load cases were then gathered or built representing each of the test series listed in Table I. Where possible, pre-existing set-ups were used to facilitate harmonisation with existing distributions (e.g. from the THUMS validation catalogue, or load case set-ups from OpenVT; Table I). The baseline biofidelity of the model was then checked in each of the load cases to check the set-up models and to verify that the HBM behaved in a reasonably biofidelic manner in each load case. This was accomplished by examining the response in a single exemplar simulation for each load case (representing the nominal input condition) for each HBM, compared to the reported PMHS response corridors describing basic kinematics and kinetics of interaction with the environment (e.g., force-deformation response corridors from the impactor tests). .

Following the initial biofidelity evaluation, matched-pair test-specific simulations were performed to expand the simulation dataset for IRF development, and to develop IRFs via regressing the HBM responses against the matched PMHS injuries. Test-specific simulations corresponded to each individual test by modifying the loading conditions, targeting the test inputs applied to the PMHS. For the impactor cases, the reported impactor velocities were applied to each test-specific simulation (Table A2, Appendix A). To account for differences in momentum transfer resulting from differences in PMHS mass, scaling was applied to the mass of the impactor hitting the HBM. The objective of this type of scaling is to expose the HBM to an impact that can be comparable to the impact received by the PMHS in the matched-pair test, and to induce comparable chest compression and injury severity between the HBM and the PMHS. In this scaling, geometrical similarity, identical density and stiffness of the thorax was assumed between the PMHS and the HBM, same as equal-stress equal-velocity scaling [22]. The impactor mass was scaled such that the initial momentum of the impactor relative to the total body mass of the subject is equal for the HBM and matched-pair PMHS test. The scaled impactor mass is given by Equation 1:

$$m_{scaled} = m_{test} \times \frac{M_{HBM}}{M_{PMHS}} \tag{1}$$

where $m_{scaled}$ is the matched-pair simulation impactor mass, $m_{test}$ is impactor mass in matched-pair test, $M_{HBM}$ is the HBM total body mass and $M_{PMHS}$ is the matched-pair PMHS total body mass. The test and scaled impactor masses for simulations with THUMS v4.1 are given in Appendx C. The THUMS mass of 75.13 kg was applied for all PMHS cases. This exercise increases the impactor simulation dataset to 88 total matched-pair simulations.

Finally, a series of sled-style simulations was performed to generate data to check the general predictive capability of the tuned IRFs. These were typically characterised by whole PMHS subjected to a lateral impact crash pulse, via an impacting wall or environment representing the interior of a vehicle. The responses of the HBMs were compared against the PMHS responses for general biofidelity assessment. The model-specific IRFs were then used to compare the injury prediction of each HBM against the injuries observed in the PMHS, to determine if the model-specific IRFs succeeded in producing harmonised injury prediction in whole-body cases that were not included in their tuning.

### *Injury Risk Function Development*

A total of 88 test-specific impactor simulations in lateral loading were performed to develop IRFs. The maximum principal strain (MPS) was calculated for each rib as the input parameter to the IRF. MPS was based on the 95th percentile peak response to avoid potential numerical issues (e.g. artefactual stress concentrations) associated with using the 100th percentile value [23-24]. By focusing on the maximum values, the MPS95 strains naturally included only the tensile (positive) strain components (unlike some other past studies, where the absolute value of the strain had been explored). This option was chosen because cortical bone exhibits higher strength and stiffness under compressive loading than under tensile loading [25-26]. However, most HBMs utilise isotropic materials with the same properties in tension and compression [27-28]. Due to the nonlinearity of real bone material strength, it may be more appropriate to consider just the tensile strain (as opposed to the absolute value of the tensile and compressive strain) when predicting rib fracture risk in cortical bone.

For each of these simulations, the injury information in terms of rib fractures sustained in the corresponding PMHS test was available from the reference literature. The Abbreviated Injury Scale (AIS) defines any occurrence of three or more rib fractures (unilateral or bilateral) to be representative of AIS3+ rib cage injury [29]. This injury level has been used to develop thoracic IRFs for the THOR ATD [30]. Previous studies have also considered an occurrence of seven or more rib fractures in PMHS tests to be representative of AIS3+ rib cage injury [31-32]. However, in PMHS and in living humans, as ribs begin to break, the internal load is transferred to the surrounding ribs, eventually compromising the overall structural stability of the chest. This phenomenon is not replicated in these simulations, as the probabilistic rib fracture prediction approach is implemented without any loss of structural integrity in the ribs. Hence, AIS3+ injury was selected for developing thoracic IRFs in this study, as it represents a lesser number of fractures and thus is less likely to be prone to biofidelity limitations from cascading fractures. For each of the 88 reference tests used in this study, the rib fracture information was converted into binary outcomes for the one level (3+ rib fractures).

The IRF tuning methodology followed the same general workflow as that of [1]. For each simulation, the predicted risk of fracture in each individual rib was calculated using a draft version of the local IRF, beginning with the age-dependent rib cortical bone ultimate strain distribution of [33] with the Weibull formulation of Equation 2 (note that the broader study surrounding [1] also explored other distributions, finding that Weibull exhibited the best fit). The risks calculated for each individual rib were then combined into a joint probability of three or more fractured ribs using a Poisson's distribution algorithm [5]. This process was repeated across all tuning simulations, resulting in a prediction of three or more fractured ribs for each test-matched simulation. These predictions were then compared to the occurrence of three or more fractured ribs in each matched test, via calculating the total negative log-likelihood summed across all of the simulations. The draft IRF was then modified by changing the $\beta_0$ and $\beta_1$ coefficients (keeping the alpha parameter constant), and the process was repeated using an optimisation routine (using the Matlab R2024b Global Optimization Toolbox) seeking to find the beta coefficients that resulted in the lowest summed negative log-likelihood.

$$Weibull\ risk\ (strain, AGE) = 1 - exp\left( - \left( \frac{strain}{exp(\beta_0 + \beta_1 \cdot AGE)} \right)^{\alpha} \right) \qquad (2)$$

This process was performed for both the THUMS v.4.1 and the GHBMC v6.0. The optimisation process was performed using just the lateral impact dataset described here, just the 170 frontal impact dataset described by [1], and the two datasets combined (for a total of 258 test-specific simulations). The IRF fit and predictive ability was further examined via reliability plots (with both the fitting data and the independent sled test simulation results) to compare the predictions from the final fitted IRFs to the proportion of tests exhibiting 3+ fractured ribs in each load case. Finally, various degrees of strain filtering (e.g. 100th percentile MPS, 95th percentile MPS, …, down to 80th percentile MPS) were examined to observe the effect on the resulting fit of the IRFs.

## III. RESULTS

Simulation environments were gathered or built for the 15 load cases (10 impactor, fice sled) shown in Table I. Both the THUMS v.4.1 and GHBMC v.6.0 showed reasonable biofidelity in all load cases compared to the available PMHS data from the literature. Therefore, the HBMs were not changed prior to fitting the IRFs. The impactor load cases were then modified to represent each of the 88 PMHS impactor tests. The resulting strain output values were used to predict the rib fracture risk for each PMHS test (including age of the PMHS), and the process was iterated to tune frontal, lateral, and combined IRFs for each HBM.

### *Injury Risk Function Development*

The optimised MPS95 strain IRFs for THUMS v4.1 and GHBMC v6.0 are shown in Fig. 1 and Table II. Consistent with the findings from the prior CRSC frontal IRFs, these lateral IRFs are shifted to the left relative to the PMHS cortical bone coupon curve, which means higher risk of rib fractures at the same level of strain (Table II and Fig. 1). Moreover, the THUMS curves are positioned further to the left compared to the GHBMC curves in each loading case.

Figure 2 shows how IRFs vary with different ages. The ages of 44, 64, and 84 years were selected to represent +/- 20 years from 64 years, the average age of PMHS in the combined frontal and lateral loading case data. Figure 3 illustrates the age effect by plotting the MPS95 strain value associated with a 50% risk of rib fracture for the front, side, and combined versions of the IRF (compared to the PMHS rib ultimate strain coupon data of [33]). To place this in context, the distribution of PMHS in our frontal- and side-impact training datasets is shown in Fig. 4. Note that [1] mistakenly described similar curves as based on MPS 95 when they were in fact based on MPS 100, and are thus not directly comparable to the curves presented here (this has since been clarified in an erratum).

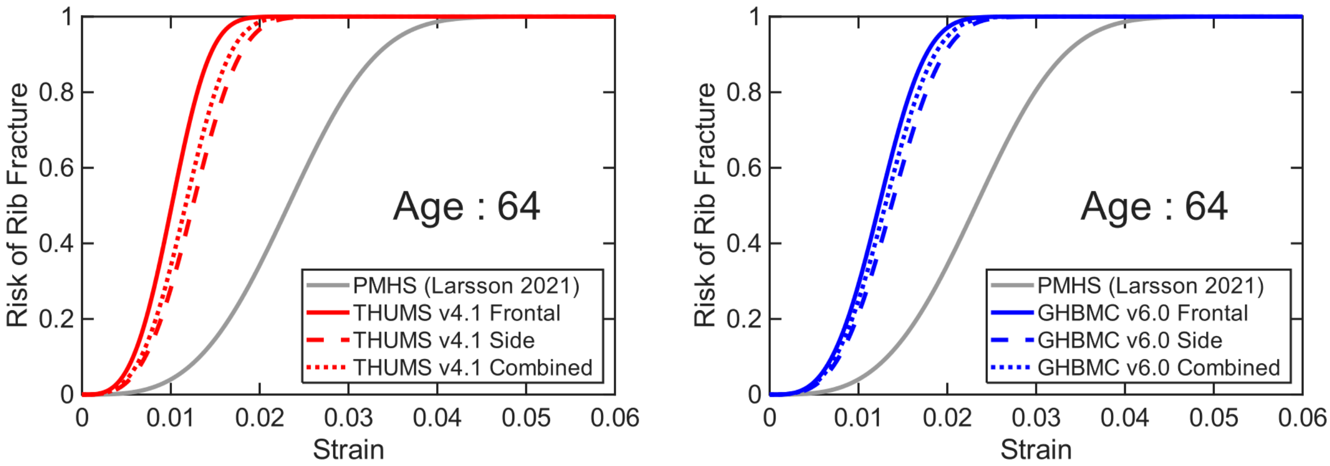


Fig. 1. Comparison of frontal, lateral, and combined IRFs for both HBMs for age 64 years old (based on MPS95 tensile strain).

TABLE II
PARAMETERS TUNED FOR THUMS V4.1 AND GHBMC V6.0 USING WEIBULL DISTRIBUTION (BASED ON MPS95 TENSILE STRAIN)

| | β0 (optimised) | β1 (optimised) | α (from Larsson 2021 [33]) |
|---|---|---|---|
| PMHS (Larsson 2021 [33]) | -2.9236 | -0.0114 | 3.3562 |
| THUMS v4.1, 3+ Fx, Frontal | -3.84176 | -0.01007 | 3.3562 |
| GHBMC v6.0, 3+ Fx, Frontal | -3.64109 | -0.0101 | 3.3562 |
| THUMS v4.1, 3+ Fx, Lateral | -2.28625 | -0.03108 | 3.3562 |
| GHBMC v6.0, 3+ Fx, Lateral | -2.58437 | -0.02494 | 3.3562 |
| THUMS v4.1, 3+ Fx, Combined | -2.91049 | -0.02239 | 3.3562 |
| GHBMC v6.0, 3+ Fx, Combined | -3.21057 | -0.01598 | 3.3562 |

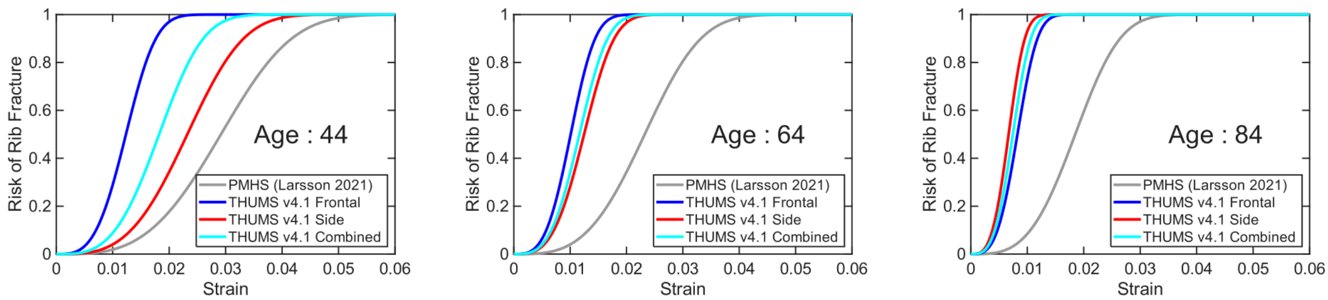


Fig. 2. Calibrated IRFs across ages 44, 64, and 84 years (based on MPS95 tensile strain).

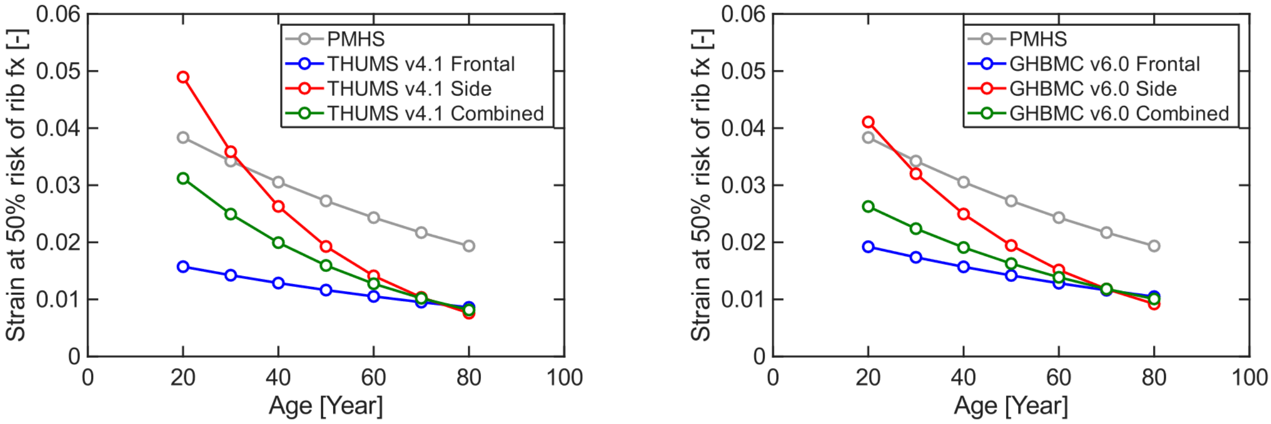


Fig. 3. Strains predicting 50% risk of 3+ rib fractures across ages 20–80 years ("PMHS" is the failure model from cortical bone coupon tests described by [33]).

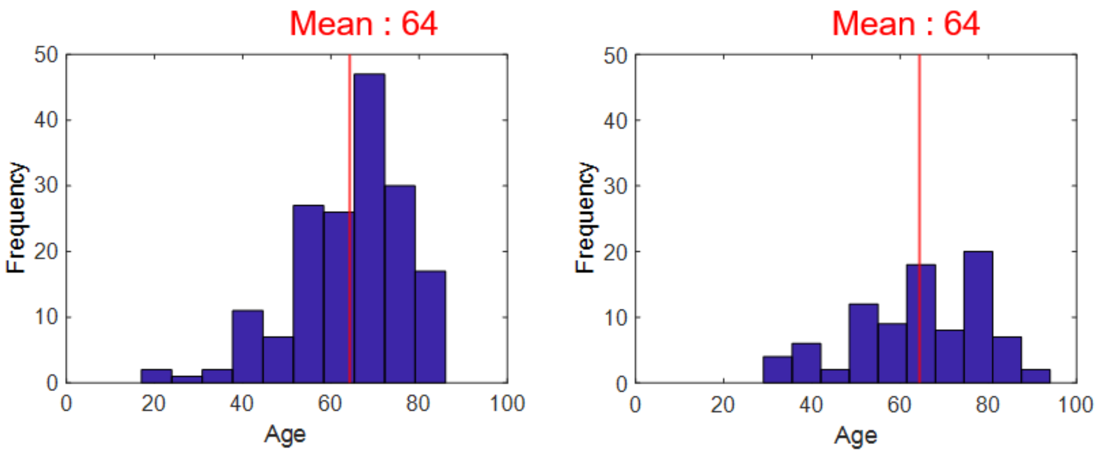


Fig. 4. Age distribution for PMHS tests for both frontal (*left*, 170 tests) and lateral (*right*, 88 tests) loadings.

***Reliability Analysis***

The reliability diagrams in Fig. 5 show the predicted risk of 3+ rib fractures using MPS95 tuned solely from the frontal cases, compared to the proportion of observed test subjects that exhibited 3+ rib fractures in those frontal load cases [1]. The blue circles are load cases that were used in the tuning of the local strain-based failure functions (the impactor and table-top cases); the diameter indicates the number of tests in each load case. The pink circles are sled load cases that were not used in the model tuning. Figure 6 shows a similar type of plot, but with the predictions from IRFs tuned solely from the side-impact cases (compared to the side-impact PMHS test subjects observed with 3+ rib fractures). Finally, Fig. 7 shows reliability plots for the IRFs tuned with the combined dataset of the frontal and side cases, applied in a unified fashion to predict the risk in both the frontal-impact and side-impact load cases. The jointly-optimized reliability diagram is also shown in Figure A12 in the Appendix, annotated with reference information to aid in observing the types of cases that tended to result in over-prediction, under-prediction, or consistent prediction.

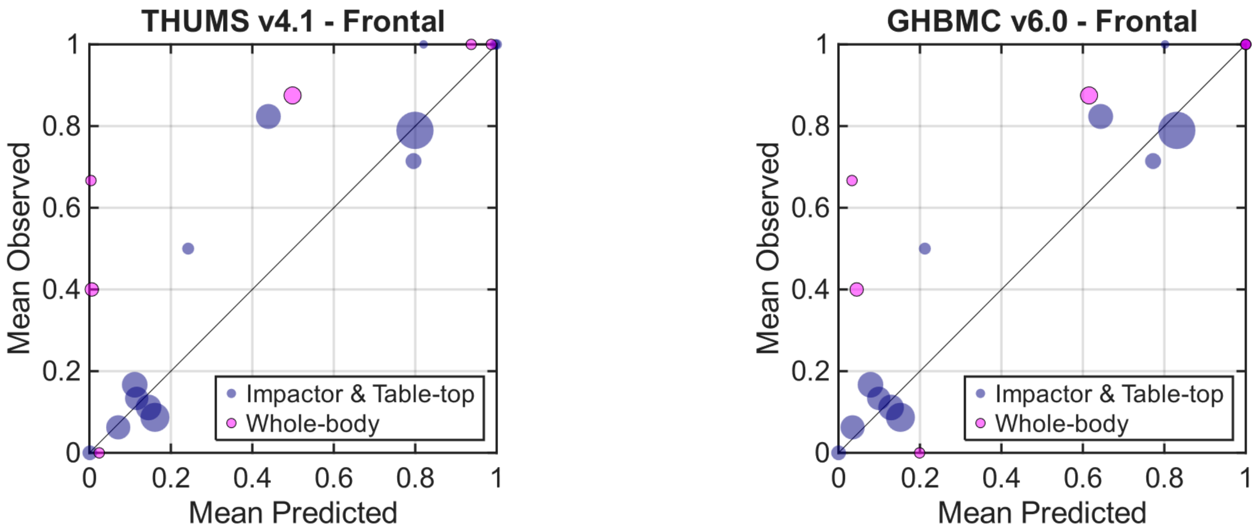


Fig. 5. Reliability diagrams for 3+ rib fractures with Independently Optimised Weibull fracture risk functions in frontal loading cases [1].

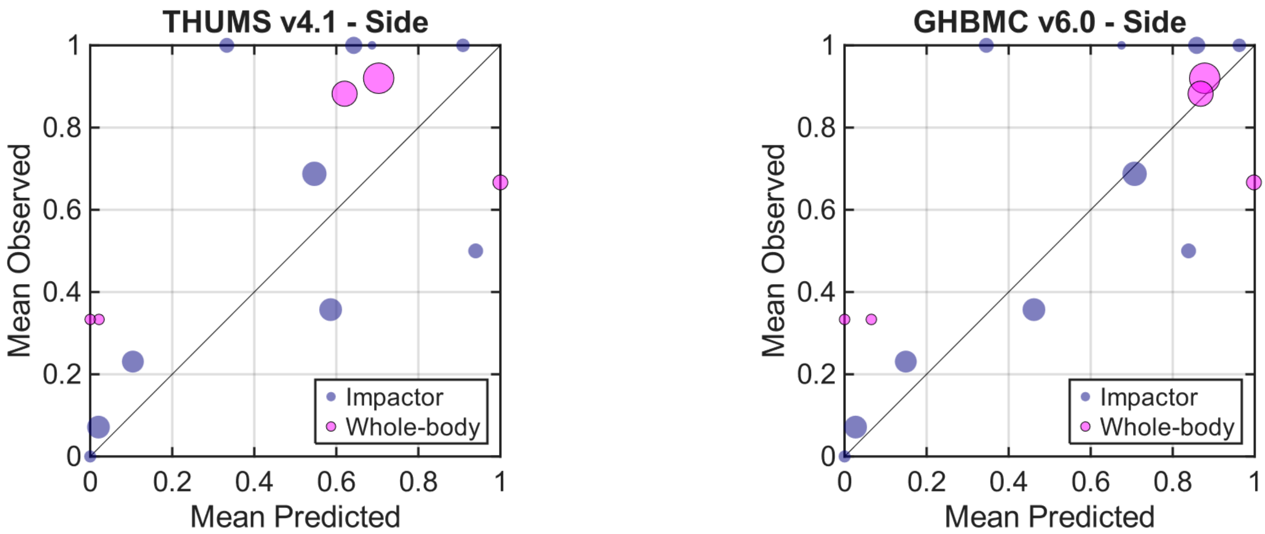


Fig. 6. Reliability diagrams for 3+ rib fractures with Independently Optimised Weibull fracture risk functions in side-impact loading cases.

***Assessment of MPS Thresholds for Rib Fracture Risk***

Lastly, although MPS95 formed the core of the analyses above, the effects of the choice of MPS threshold were also studied. The objective function values were compared across different thresholds (after refitting the IRF for each level of MPS). As above, the summed negative log-likelihood was used as the objective function for this analysis. With regular log-likelihood, the value is generally negative and a higher value suggests a better fit. To simplify the interpretation, in this study the sign of the log-likelihood was flipped (hence the use of negative log-likelihood) so that the output values are positive, and a smaller positive value indicates a better fit. Thus, the optimal MPS threshold should have the smallest objective function value. The data from frontal loading scenarios alone [1] were used because the frontal dataset contains a larger and more balanced sample than the lateral dataset. The results of refitting the IRF using the frontal impact dataset across different MPS percentile values are shown in Fig. 8.

The objective function value demonstrated a flat zone between MPS95 and MPS99, particularly for GHBMC v6.0. MPS95 has been widely used in brain injury research [23-24] to avoid numerical issues with MPS100. In line with this practice, our analysis supports adopting MPS95 as the predictor for rib fracture risk, as there was little overall change below MPS100 (with a slight improvement in fit as we move toward MPS95 for THUMS).

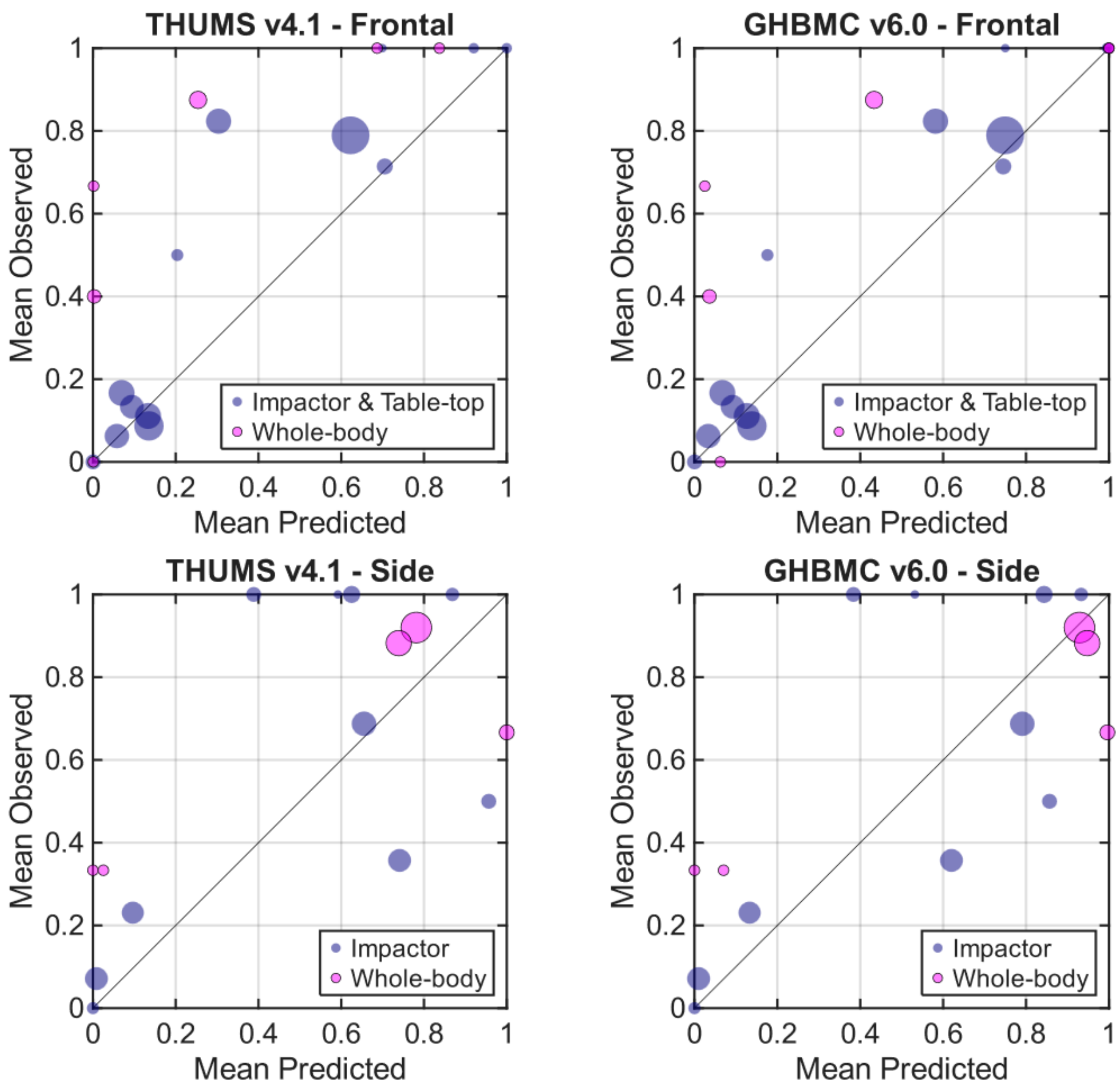


Fig. 7. Reliability diagrams for 3+ rib fractures using combined IRFs in frontal and side-impact loading cases, respectively.

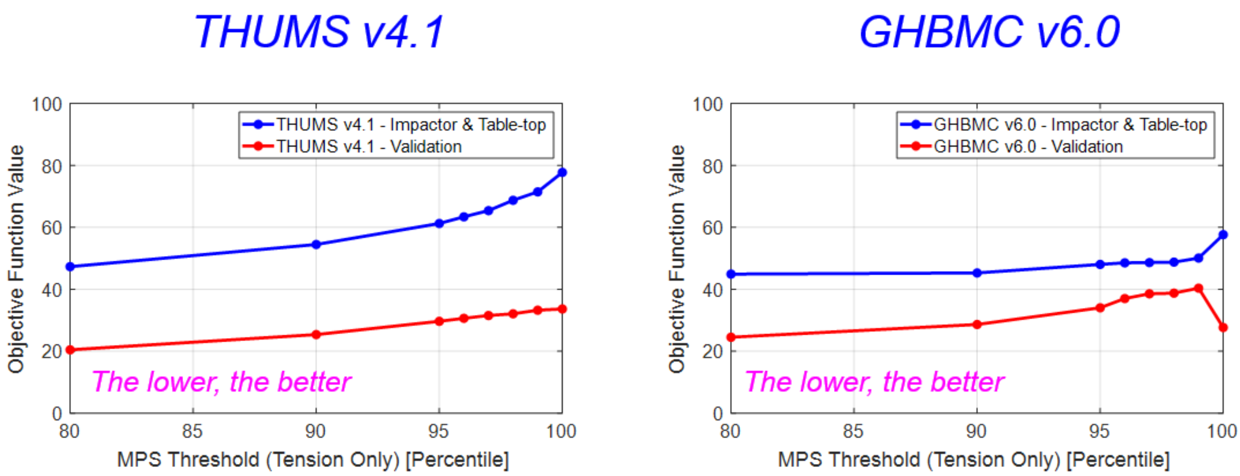


Fig. 8. Objective function values for predicting 3+ rib fractures across different MPS thresholds from MPS80 to MPS100 for THUMS v4.1 and GHBMC v6.0.

## IV. DISCUSSION

This study evaluated whether 3+ rib fracture probability can be represented using a single strain-based IRF across frontal and lateral loading conditions. Historically, separate IRFs for frontal and lateral loading were appropriate given differences in dummy hardware and measurement techniques. Global measures such as deflection or acceleration required direction-specific tuning to account for differing thoracic engagement patterns. However, strain-based metrics extracted from HBMs represent local deformation within cortical bone. Provided that strain is computed using consistent anatomical definitions and numerical procedures, the mapping between strain magnitude and fracture probability should not depend on the direction of the global loading vector. The unified IRFs developed here demonstrated predictive performance comparable to loading-specific formulations while avoiding this directional dependency. This verifies that, when tuned with sufficient data spanning the loading modes of interest, it is possible to develop and validate HBM-specific IRFs that are broadly applicable across a range of loading directions.

It is important to note that harmonisation of the probabilistic strain–fracture relationship does not imply that frontal and lateral impacts produce identical thoracic injury mechanics. Global kinematics, rib engagement, and load distribution may vary substantially with impact direction. These differences influence injury risk through their effect on computed strain distributions. The present work does not suggest that loading mode is irrelevant; rather, it suggests that the probabilistic injury tolerance for the region may be represented consistently using local strain. The key is that the HBM must be sufficiently biofidelic across a range of loading modes so that the relationship between global loading mechanisms and the local strain field may be reasonably captured. If the HBM is selectively biofidelic, with biofidelity limitations that are dependent on loading mode, then this would likely manifest as a deviation in the relationship between rib strain and perceived injury risk. There is currently no established method to evaluate strain-field biofidelity across a range of loading modes. Instead, the best that we can do is investigate the consistency of the relationship between predicted strain and injury risk. The consistency in this relationship (independent of loading mode) may be one surrogate means to evaluate the biofidelity and/or practical range of suitability of the HBM. Thus, the load case catalog and evaluation methodology described may provide a means to assess not only the mechanical biofidelity against a range of load cases but also the general universality of biofidelity and injury risk prediction capability of the HBM.

### *Age Effects*

A notable difference between the frontal- and side-impact curves is that absolute $\beta0$ values for the side curves in both HBMs are lower than those of the frontal curves, whereas the absolute $\beta1$ values for the side curves are higher compared to the frontal curves. The difference in $\beta1$ values indicates that the age effect is stronger in the side-impact cases in this dataset. This resulted in the front, side, and combined IRFs for the THUMS v4.1 model differing substantially at age 44, but becoming more similar as age increases; at age 84, the three THUMS IRFs for the frontal, lateral and combined nearly overlap. Further, the frontal and combined datasets tend to exhibit age effects most similar to the IRF derived by [33], while the side-impact IRFs tend to exhibit stronger age-related effects (Fig. 3). The IRF developed by Larsson *et al*. [33] is based on rib cortical bone coupon tests performed on a relatively large PMHS dataset (58 subjects) spanning a wide age range (17–99 years), providing broad coverage of both subject count and age distribution. The unique behaviour of the side-impact IRFs in the present study likely resulted from fewer data points for side-impact cases, especially at younger subject ages. The limited sample size (88 data points compared to the 170 frontal loading cases) combined with the skewed distribution toward older subjects (Fig. 4) may have reduced the comparative accuracy of the IRFs at younger ages and contributed to the apparent age effects. Therefore, it is possible that the IRF may most accurately represent injury risk for occupants around age 64 and older, and may lose accuracy for occupant ages substantially below those of the underlying data. Furthermore, the frontal and side IRFs bracket the slope (age sensitivity) of the Larsson IRF, with the combined IRF most closely matching the Larsson formulation [33]. This suggests that when the datasets are combined (effectively increasing both the sample size and the age diversity of the underlying data), the estimated age effect tends to converge toward a similar solution. This highlights the importance of contextualising the expected accuracy of the IRFs considering the strengths and weaknesses of their underlying data when interpreting their predictions, regardless of application.

As a result, we have the highest confidence in the fidelity of the IRFs from around age 55 and older, as that is where most of the underlying data lie. The fact that there is limited sensitivity to loading direction in this age range (where we have the most confidence in the IRF) suggests that there may be limited sensitivity to loading direction overall. The divergence at younger ages may very well be caused by a lack of data to properly inform the IRF in that range. As the combined IRF captures the limited directional sensitivity at older ages (where we have the most data) and captures an “average” risk at younger ages (while using the entirety of the limited data available to inform prediction in that range), we recommend that the combined functions be used for all directions and age ranges.

***Reliability Analysis***

In the frontal loading cases, both models have reasonable ability to discriminate between events that have a very high risk of injury, compared to events that have a very low risk of injury (Fig. 5). The greatest differences were observed in the transition region in three sled cases where both models appeared to underpredict injury risk. This observation likely reflects the challenge of evaluating a model using a small number of PMHS tests as opposed to systematic model bias. Additional data collection should focus on the transition region for injury risk to improve the fidelity of discriminating finer differences in risk.

We applied the same analysis to the lateral loading case, using the IRFs tuned solely from the lateral cases (Fig. 6). Consistent with the frontal loading results, the lateral IRFs generally discriminated the incidence of 3+ rib fractures. Although some impactor cases used in the optimisation process deviate from the prediction line, the whole-body sled cases (not included in the IRF tuning) were predicted reasonably. One potential explanation for the deviation is that certain impactor cases involved prescribed motion with a stroke limit (as opposed to fixed energy/momentum transfer). In such cases, factors such as HBM construction, rib geometry, and HBM posture may have prevented the impactor from engaging the thorax to the same severity as the tests. Despite these differences, the IRF tuning process effectively distinguishes high-risk from low-risk scenarios.

One potential advantage of strain-based injury prediction methods is their applicability across diverse loading modes. As shown in Fig. 2 and Fig. 3, the individually optimised IRFs for frontal and lateral loading differ at younger ages but converge with increasing age. As an alternative approach, the combined IRFs were optimised jointly with the combined dataset of the frontal and lateral cases. As shown in Fig. 1, the combined IRFs lie between the individually optimised functions. Although jointly optimising increased some deviation from the underlying data (because we are removing a degree of freedom from the model), Fig. 7 demonstrates that the combined models still provide reasonably good discriminative ability across the dataset (for both the frontal and lateral impact directions). In fact, improvements were observed in the sled cases under lateral loading, suggesting that in some cases the benefit of including additional data outweighed the reduced degrees-of-freedom of the model.

***MPS Thresholds***

There has been a recurring discussion in the literature of the most appropriate means to output and process rib strain for injury risk prediction. The most important thing is that a particular rib strain processing method is applied consistently when tuning an IRF and when employing the tuned IRF. Secondary to that, there are many different options, including using tensile strain only, tension and compression strain, and various levels of filtering (i.e. MPS percentile levels). The results here demonstrate that when using the tensile MPS95, unified IRFs can be tuned for the THUMS v.4.1 and GHBMC v.6.0 that work well in both frontal and side impact. (Note: the MPS95 IRFs tuned here are quite different from those previously described by [1] – the present study is intended to supersede the prior work, which now includes an erratum.)

MPS95 is a commonly used strain-filtering threshold, representing a compromise between preserving information and filtering out potential high-strain modelling artifacts. For example, it has been widely used for brain modelling [23-24] to avoid numerical issues with MPS100. As shown in Fig. 8, the choice of MPS filtering value does affect the fit of the resulting IRFs. Figure 8 shows that a flat zone appeared between MPS95 and MPS99, particularly for GHBMC v6.0. Even though the sum negative log-likelihood continues to show improvement with more aggressive strain filtering, the improvement is small compared to the initial improvement when moving from MPS100 to MPS95. More aggressive filtering removes additional information, which may be important in some cases. To compromise between mitigating the potential influence of strain artifacts while preserving available information, our analysis supports adopting MPS95 as the predictor for rib fracture risk, as there is little overall change below MPS100.

### *Limitations and Future Directions*

Several limitations warrant discussion. First, available datasets were not originally designed for cross-mode harmonisation, and differences in testing modes, age distribution, and specimen screening criteria may influence observed strain–injury relationships. In addition, there were some testing modes where the same PMHS were subjected to multiple tests (e.g., [6]). These were included to make use of all available data, and although they comprise a relatively small portion of the overall dataset the potential influence of repeated impacts remains uncertain. This dataset also included wide range of PMHS (including both males and females) that likely exhibited a wide range of bone strength and fragility. This was intentional, as the hope is that the tuned IRF may be able to tell us something about the risk of injury to the population (or at least the population represented by these PMHS). We want the IRF to include information capturing a wide range of fragility, so that the risk predicted includes consideration for the more fragile segments of the population.

Second, the predicted strain magnitude depends on HBM fidelity, mesh resolution, and material formulation. The unified IRFs are therefore conditional to the modelling framework used to compute strain. When applying model-tuned IRFs, care should be taken to ensure that strain is processed in a manner consistent with the method used in the IRF tuning. In addition, the joint probability model employed here (via the Poisson distribution) inherently assumes that each fracture is an independent event. In reality, the probability of fracture in any individual rib is likely related to the probability of fracture elsewhere in the ribcage, via the intra-subject bone strength as well as the structural integrity of the ribcage. We encourage continued investigation to study the potential implications of these effects, and the degree to which they should be considered in application-focused fracture prediction. There are also several studies that use rib cortical bone ultimate strain [33] in its raw form as a means for injury prediction, without further HBM-specific tuning [e.g., 36]. This may be entirely appropriate for some HBMs and/or applications (especially applications where harmonizations across HBMs may not be needed), as it may be reasonable to assert that different HBMs simply represent different people.

Finally, this study focused specifically on rib fracture represented by the tensile component of cortical strain. Other thoracic injury mechanisms, including soft tissue injury or costovertebral joint disruption, may not be fully captured by cortical strain alone. Even within the rib bone, there is the potential for more advanced techniques to incorporate the full triaxiality of the stress state into probabilistic fracture prediction [34,35]. Thus, the current study should not necessarily be viewed as a terminal, final answer to thoracic injury prediction with HBMs. Instead, this study simply presents and demonstrates one potential path by which a set of harmonized HBM IRFs may be developed. There may be other methods, with different strain IRF optimization paths, formulations, or methods that may improve accuracy or robustness beyond the method presented here, and we would encourage others to continue to explore such paths. Even so, extension of these prediction-focused harmonisation principles to additional injury metrics and IRF development (or validation) methods may continue to benefit from the broad-based, data-focused framework presented here.

Despite these limitations, the present findings suggest that a unified strain-based IRF is feasible and may enhance consistency in HBM-based injury prediction across loading modes. While we should still strive to ensure that HBMs behave in a robust, biofidelic manner across lengths scales, the injury prediction harmonisation method presented here represents a step toward mechanism-agnostic injury assessment in multi-directional crash evaluation - a future potential strength of HBMs.

## V. CONCLUSIONS

This study built on previous work developing a method to tune rib fracture risk functions for application to specific HBMs, extending from frontal impact to combined frontal and side impact. In all, 88 new simulations were performed across 10 impactor loading conditions, with each simulation representing a specific past test with PMHS. These were applied to the THUMS v4.1 and GHBMC v6.0 mid-sized male HBMs, developing tuned IRFs for each. The predictive ability was then validated using a series of whole-body sled test simulations that were not used in the IRF tuning. The key conclusions that can be drawn from this study are as follows.

- Both of the HBMs exhibited reasonable baseline biofidelity in the load cases investigated (with no concerns that suggested a clear need to modify the model).
- The predictive accuracy of the local, strain-based IRFs tended to improve with increased spatial filtering of the MPS (for both HBMs).
- The 95th percentile MPS (MPS95) appears to provide a reasonable balance between prediction accuracy and a desire to preserve the information provided by the strain field.
- When the local, strain-based IRFs were developed using the MPS95 (with the maximum tensile component of the strain), the IRFs developed from the side-impact PMHS tests were similar to the IRFs developed from the frontal impact tests, within the age range that formed the bulk of the PMHS data (specifically, approximately 55–80) years.
- Because of that similarity, we recommend that it is reasonable to use one jointly-fit IRF using both the frontal-impact and side-impact data. We have the greatest confidence in the predictive ability of such a jointly-fit IRF in the age range of 55–80 years. (Beyond that, the IRFs diverge due to differences in the side-impact and frontal-impact PMHS data.)
- Once the IRFs were developed using the method described above, they appeared to provide reasonable prediction in the whole-body sled test simulations that were examined, compared against reference PMHS tests.
- The above observations apply to both the THUMS v4.1 and GHBMC v6.0 50th percentile male models. The tuned IRFs are different for each, but the overall trends and predictive abilities (using their specificallytuned IRFs) are similar.

## VI. ACKNOWLEDGEMENTS

This work was funded by the Toyota Collaborative Safety Research Center (CSRC). The GHBMC human body model was used with permission from the Global Human Body Models Consortium.

## VII. REFERENCES

[1] Forman, J., Kulkarni, S., Perez-Rapela, D., Mukherjee, S., Panzer, M., & Hallman, J. (2022). A method for thoracic injury risk function development for human body models. *Proceedings of the IRCOBI Conference*, 2022. Porto, Portugal.

[2] Gepner, B. D., Perez-Rapela, D., *et al*. (2022) Evaluation of GHBMC, THUMS and SAFER human body models in frontal impacts in reclined postures. *Proceedings of the IRCOBI Conference*, 2022, Porto, Portugal.

[3] Forman, J. L., Gepner, B., *et al.* (2026) Strategies for injury prediction with human body models. *Proceedings of the 28th ESV Conference*, 2026, Toronto, Canada.

[4] Peres, A., Forman, J. L., Kent, R. W. (2016) Pelvis fracture injury risk functions for HBMs. *Proceedings of the IRCOBI Conference*, 2016, Malaga, Spain.

[5] Forman, J. L., Kent, R. W., Mertz, H. J. (2012) Rib fracture risk assessment using a probabilistic framework. *Proceedings of the IRCOBI Conference* (2012), Dublin, Ireland. [6] Viano, D. C., Lau, I. V., King, A. I. (1989) Thoracic injury biomechanics in lateral impact. SAE Technical Paper 892432.

[7] Subit, D., Duma, S. M., Crandall, J. R. (2010) Thoracic response to lateral and oblique impact. *Journal of Biomechanics,* **43**: pp. 123–131.

[8] Shaw, G., Parent, D., *et al*. (2006) Impact response of the human thorax. *Stapp Car Crash Journal*, **50**: pp. 109–146.

[9] Robbins, D. H., King, A. I., *et al.* (1979) Thoracic injury tolerance in lateral impact. SAE Technical Paper 790925.

[10] Trosseille, X., Baudrit, P., Petit, P. (2008) Biomechanics of thoracic injury in lateral impact. *Proceedings of the IRCOBI Conference,* 2008, Bern, Switzerland. [11] Leport, T., Trosseille, X., Baudrit, P., Petit, P. (2011) Thoracic injury mechanisms in lateral impact. *Proceedings of the IRCOBI Conference*, 2011, Kraków, Poland. [12] Kemper, A. R., McNally, C., Kennedy, E., Duma, S. M. (2008) Thoracic response and injury tolerance in lateral impact. *Proceedings of the IRCOBI Conference,* 2008, Bern, Switzerland.

[13] Chung, J., Cavanaugh, J. M., King, A. I. (1999) Thoracic response and injury in lateral impact. SAE Technical Paper 1999-01-0633.

[14] Compigne, S., Baudrit, P., Petit, P. (2004) Biomechanical response of the thorax in lateral impact. *Proceedings of the IRCOBI Conference,* 2004, Graz, Austria. [15] Petit, P., Baudrit, P., Trosseille, X. (2019) Far-side lateral impact sled tests. *Proceedings of the IRCOBI Conference*, 2019, Florence, Italy. [16] Lessley, D. J., *et al*. (2010) Lateral impact sled testing of PMHS. *Stapp Car Crash Journal*, **54**: pp. 321–350.
[17] Park, G., Kim, T., Crandall, J. R., Arregui Dalmases, C., Luzón Narro, B. J. (2013) Comparison of kinematics of GHBMC to PMHS on the side impact condition. *Proceedings of the IRCOBI Conference*, 2013, Gothenburg, Sweden, pp. 368–379.
[18] Park, G., Kim, T., Panzer, M. B., Crandall, J. R. (2016) Validation of shoulder response of human body finite-element model (GHBMC) under whole body lateral impact condition. *Annals of Biomedical Engineering*, **44**(8): pp. 2558–2576.
[19] Shaw, G., Parent, D., *et al.* (2014) Lateral impact sled testing with airbag interaction. *Stapp Car Crash Journal*, **58**: pp. 45–75.
[20] Maltese, M. R., Eppinger, R. H., *et al*. (2002) Side impact PMHS testing. SAE Technical Paper 2002-22-0003.
[21] Cavanaugh, J. M., Walilko, T. J., Malhotra, A., Zhu, Y., King, A. I. (1993) Biomechanical response and injury tolerance of the thorax in lateral impact. SAE Technical Paper 933127.
[22] Mertz, H. J., Irwin, A. L., Prasad, P. (2003) Biomechanical and scaling bases for frontal and side impact injury assessment reference values. SAE Technical Paper 2003-22-0009.
[23] Panzer, M. B., Myers, B. S., Capehart, B. P. (2012) Development of a finite element model of the human head. *Annals of Biomedical Engineering*, **40**: pp. 153–167.
[24] Gabler, L. F., Crandall, J. R., Panzer, M. B. (2016) Development of a metric for predicting brain injury using FE models. *Annals of Biomedical Engineering*, **44**: pp. 1235–1247.
[25] Yates, C., *et al*. (2021) Tensile vs compressive properties of cortical rib bone. *Journal of Biomechanics*, **118**: 110315.
[26] Katzenberger, M., *et al*. (2019) Mechanical behavior of rib cortical bone under dynamic loading. *Journal of Biomechanics*, 94: pp. 45–53.
[27] Iwamoto, M., Nakahira, Y., Kimpara, H. (2015) Development of a next-generation human body model. *Stapp Car Crash Journal*, **59**: pp. 345–372.
[28] Li, Z., Kindig, M. W., Kerrigan, J. R., Crandall, J. R. (2010) Rib cortical bone material properties in human body models. *Stapp Car Crash Journal*, **54**: pp. 75–98.
[29] Abbreviated Injury Scale (2015) Association for the Advancement of Automotive Medicine, Chicago, IL.
[30] Poplin, G. S., *et al*. (2017) Development of thoracic injury risk functions for the THOR ATD. *Traffic Injury Prevention*, **18**(S1): pp. S109–S117.
[31] Kent, R. & Patrie, J. (2005) Chest deflection tolerance to blunt anterior loading is sensitive to age but not load distribution. *Forensic Science International*, **149**(2–3): pp. 121–128.
[32] Laituri, T. R., Kent, R. W., *et al*. (2005) Age-related rib fracture tolerance. *Stapp Car Crash Journal*, **49**: pp. 123–142.
[33] Larsson, J., *et al*. (2021) Age-dependent ultimate strain distribution of human rib cortical bone. *Journal of the Mechanical Behavior of Biomedical Materials*, **115**: 104287.
[34] Cronin, D. S., Watson, B., Khor, F., Gierczycka, D., & Malcolm, S. (2022). Cortical bone continuum damage mechanics constitutive model with stress triaxiality criterion to predict fracture initiation and pattern. Frontiers in Bioengineering and Biotechnology, 10, 1022506.
[35] Corrales Fabre, M. A., Cronin, D. (2026). Thorax Response in Young and Aged Small Females Under Side Impact, Isolated Ribs and Full-Body Computational Studies. Short Communication. Proc. 28th International Technical Conference on the Enhanced Safety of Vehicles.
[36] Pipkorn, B. (2026). Assessing Injury Prediction with Human Body Models: Application to Rib Fracture Risk Prediction Using SAFER HBM. SAE International Journal of Transportation Safety, 14(1).

# VIII. APPENDIX

### *Appendix A: Illustrations and Details of the Loadcases Simulated in this Study*

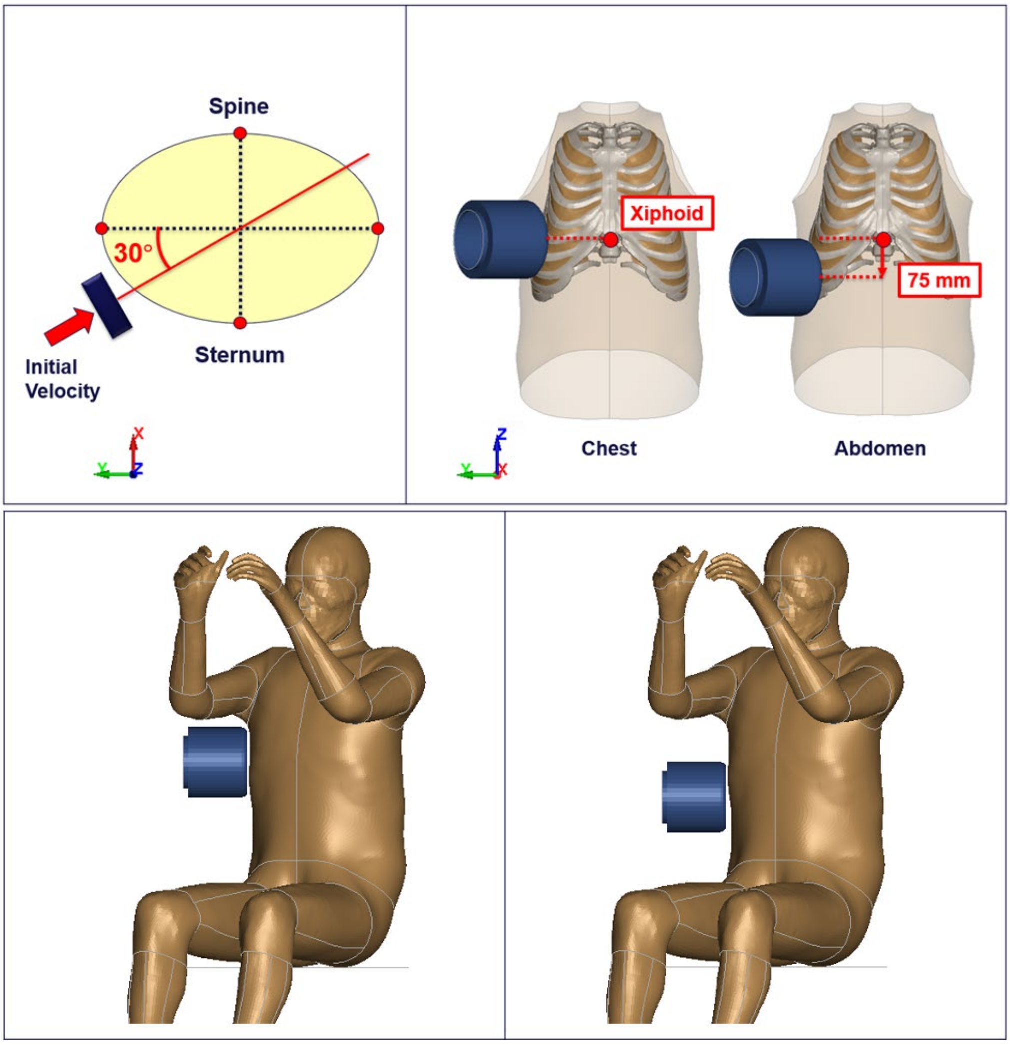


Fig. A1. Hub impactor cases of Viano *et al.* [6].

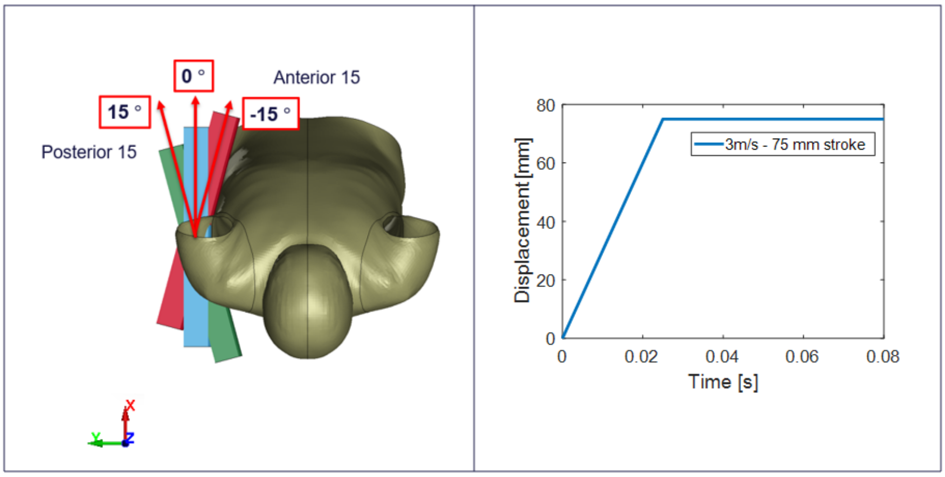


Fig. A2. Stroke-limited bar impactor cases of Subit *et al.* [7].

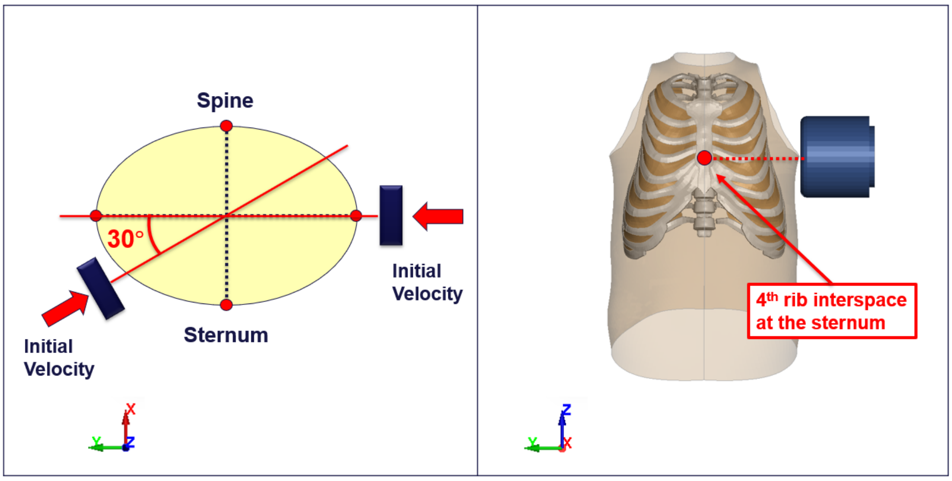


Fig. A3. Hub impactor cases of Shaw *et al*. [8].

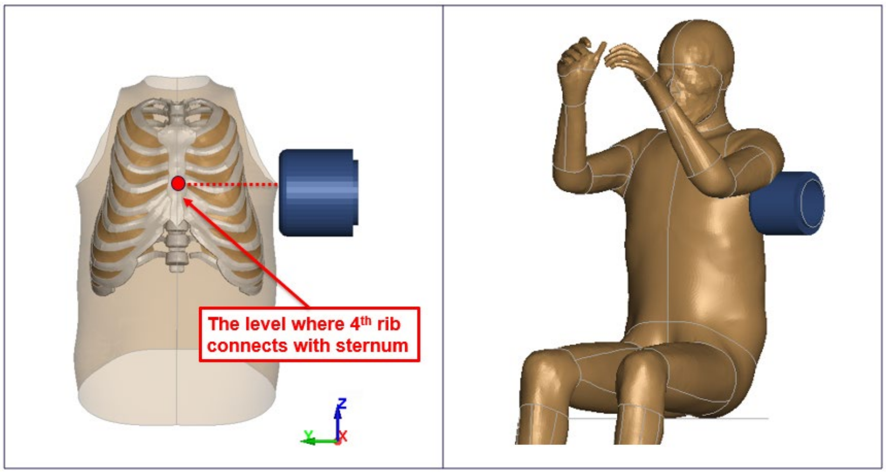


Fig. A4. Hub impactor cases of Robbins *et al.* [9].

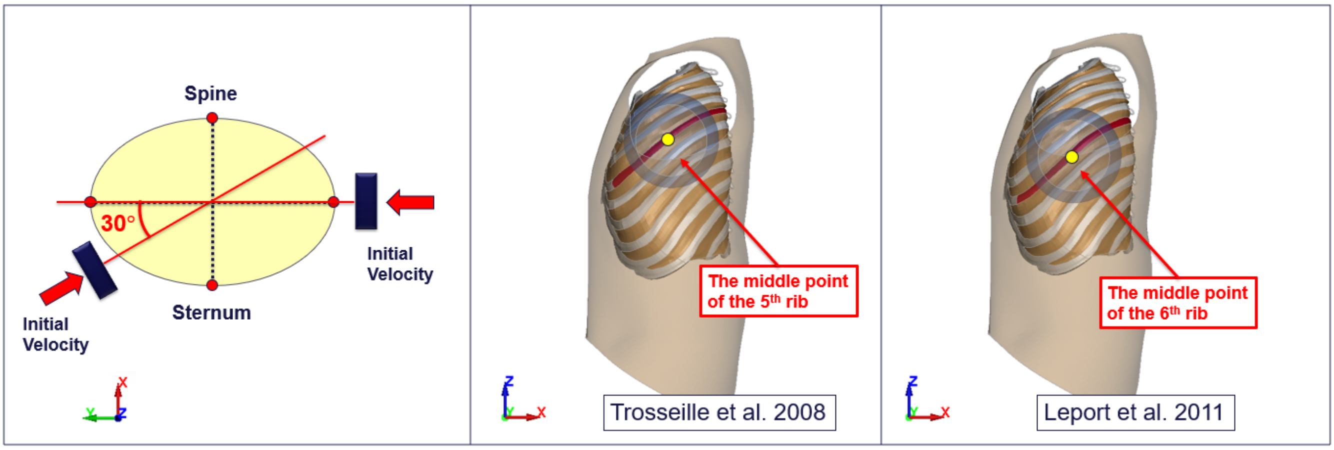


Fig. A5. Hub impactor cases of Trosseille *et al.* [10] and Leport *et al*. [11].

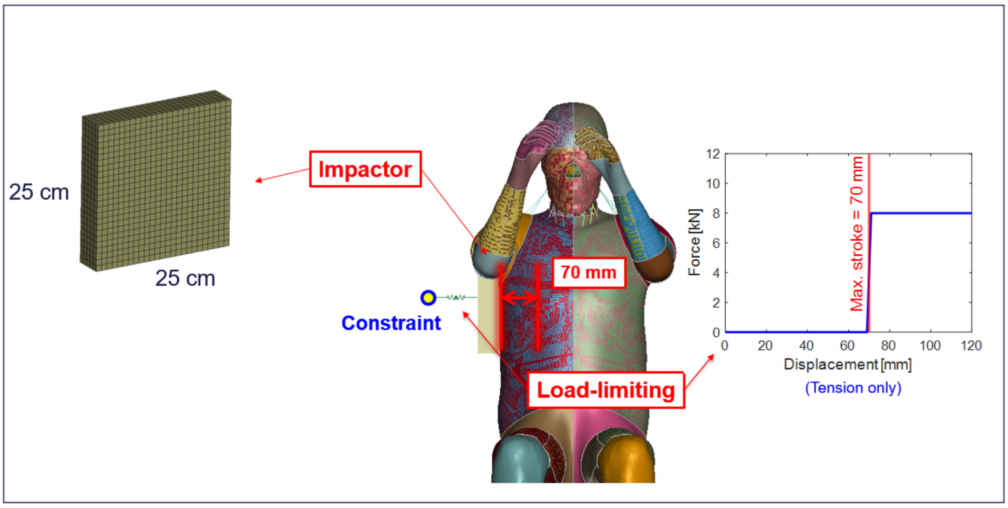


Fig. A6. Flat plate impactor cases of Kemper *et al*. [12] (with a stroke limit accomplished via a load-limiting spring that dropped the applied force after the specified stroke limit).

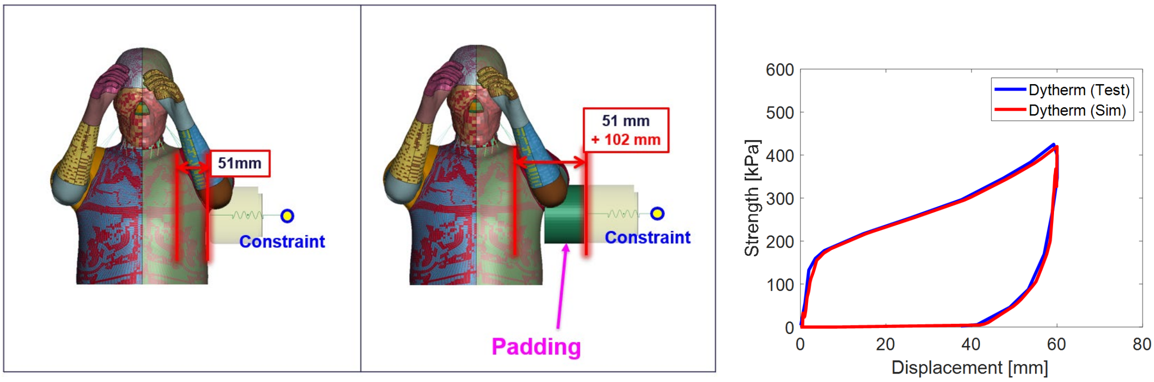


Fig. A7. Rigid hub impactor cases and padded impactor cases of Chung *et al*. [13].

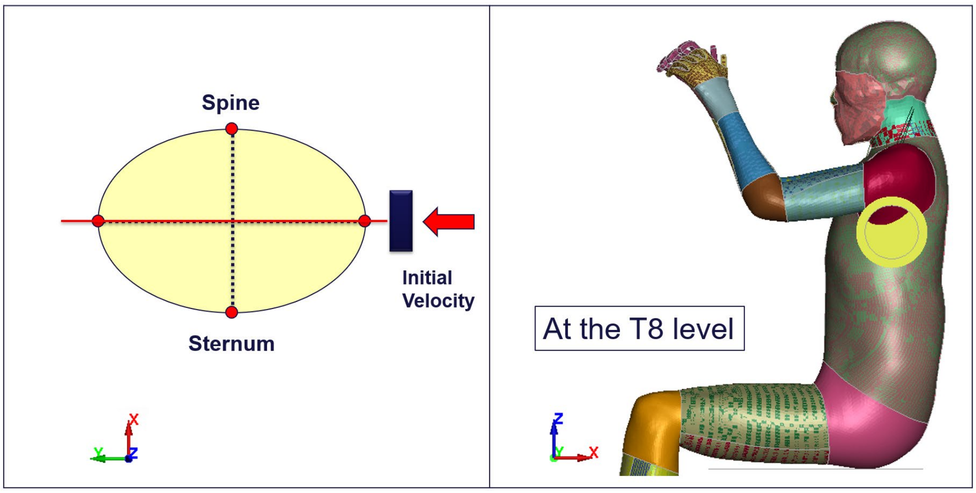


Fig. A8. Rigid hub impactor cases of Compigne *et al*. [14].

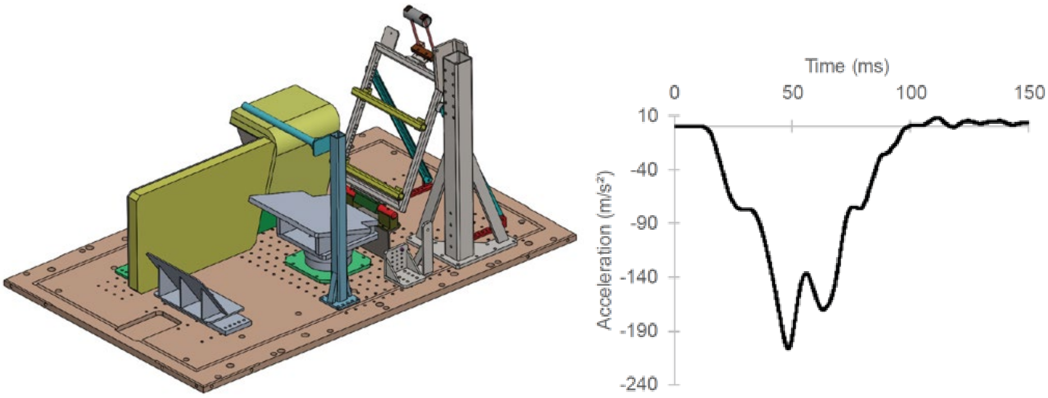


Fig. A9. Far-side sled set-up of Petit *et al.* [15].

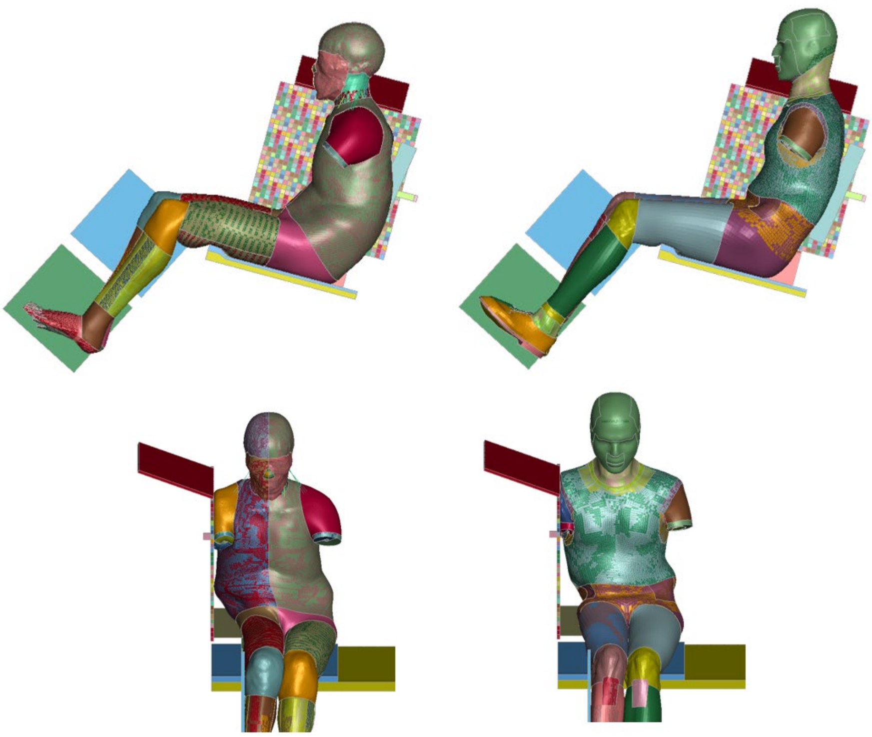

Fig. A10. Offset rigid wall sled set-up of Lessley *et al*. [16] with the THUMS v4.1 (*left*) and GHBMC v6.0 (*right*). The bottom images show engagement 20 ms into the simulation (illustrating differences in the geometry of the HBMs).

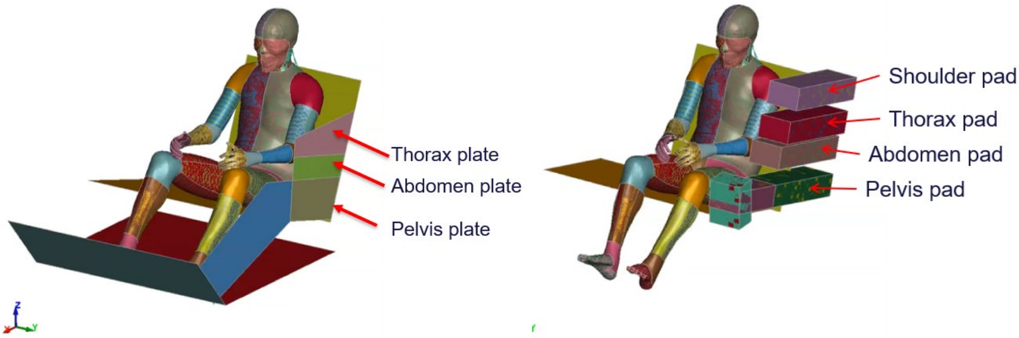


Fig. A11. *Left*: rigid wall sled set-up of Maltese *et al*. [20]. *Right*: padded wall sled set-up of Cavanaugh *et al.* [21].

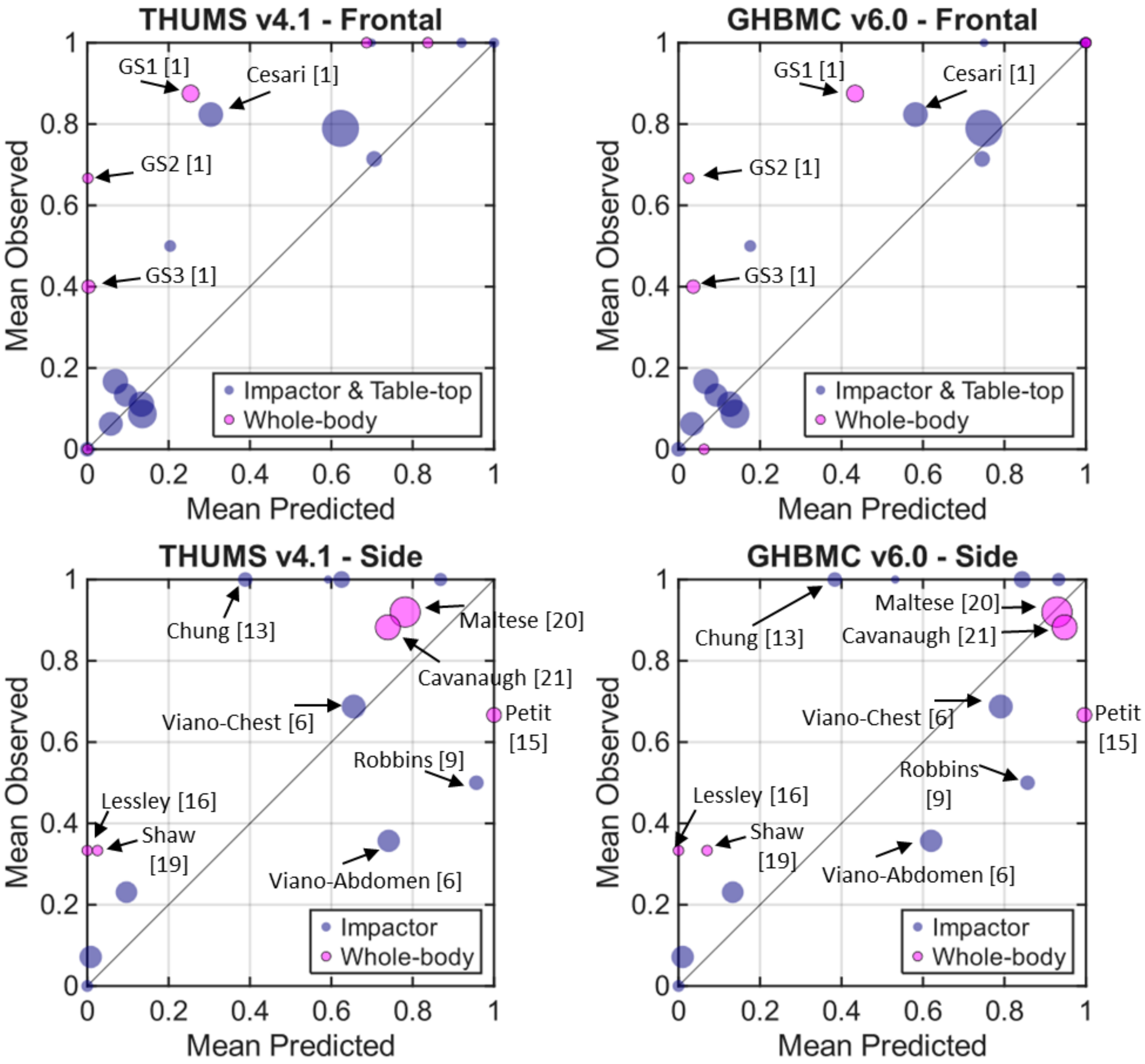


Figure A12: Reliability diagrams for 3+ rib fractures using combined IRFs in frontal and side-impact loading cases, respectively, annotated to label select specific load cases.

***Table A1: PMHS Details and Injury Information for All Side Impact Tests***

| Ref. | PMHS_ID | Test_ID | Age | Sex | Height (cm) | Weight (kg) | Total Rib Fractures | 3+ Rib Fractures |
|---|---|---|---|---|---|---|---|---|
| Viano 1989 [6] – Chest | 863 | 2 | 49 | M | 176.0 | 107 | 14 | 1 |
| | RNY1 | 3 | 76 | F | 153.5 | 44 | 19 | 1 |
| | 935 | 4 | 63 | M | 174.0 | 69.85 | 7 | 1 |
| | 947 | 5 | 38 | M | 166.5 | 56.25 | 3 | 1 |
| | 954 | 7 | 66 | M | 159.0 | 56.25 | 6 | 1 |
| | RNY2 | 9 | 64 | M | 171.0 | 61.69 | 5 | 1 |
| | 956 | 11 | 40 | F | 175.0 | 76.2 | 5 | 1 |
| | 993 | 14 | 49 | M | 173.0 | 70.76 | 9 | 1 |
| | 986 | 17 | 29 | M | 173.0 | 70.3 | 0 | 0 |
| | 986 | 18 | 29 | M | 173.0 | 70.3 | 10 | 1 |
| | 8 | 29 | 52 | F | 157.0 | 53.07 | 0 | 0 |
| | 8 | 33 | 52 | F | 157.0 | 53.07 | 12 | 1 |
| | U0M1 | 36 | 37 | M | 186.5 | 67.59 | 0 | 0 |
| | U0M1 | 37 | 37 | M | 186.5 | 67.59 | 15 | 1 |
| | U0M2 | 40 | 64 | M | 178.5 | 75.76 | 2 | 0 |
| | U0M2 | 41 | 64 | M | 178.5 | 75.76 | 0 | 0 |
| Viano 1989 [6] – Abdomen | 947 | 6 | 38 | M | 166.5 | 56.25 | 4 | 1 |
| | 954 | 8 | 66 | M | 159.0 | 56.25 | 7 | 1 |
| | RNY2 | 10 | 64 | M | 171.0 | 61.69 | 0 | 0 |
| | 956 | 12 | 40 | F | 175.0 | 76.2 | 2 | 0 |
| | 993 | 15 | 49 | M | 173.0 | 70.76 | 0 | 0 |
| | 986 | 19 | 29 | M | 173.0 | 70.3 | 0 | 0 |
| | 986 | 20 | 29 | M | 173.0 | 70.3 | 9 | 1 |
| | 47 | 23 | 62 | M | 176.5 | 83.91 | 0 | 0 |
| | 47 | 24 | 62 | M | 176.5 | 83.91 | 0 | 0 |
| | 47 | 28 | 62 | M | 176.5 | 83.91 | 0 | 0 |
| | 8 | 30 | 52 | F | 157.0 | 53.07 | 0 | 0 |
| | 63 | 34 | 64 | M | 173.0 | 48.54 | 6 | 1 |
| | U0M2 | 42 | 64 | M | 178.5 | 75.76 | 1 | 0 |
| | U0M2 | 43 | 64 | M | 178.5 | 75.76 | 4 | 1 |
| Subit 2010 [7] | S1 | 1 | 79 | M | 181 | 79 | 0 | 0 |
| | S1 | 2 | 79 | M | 181 | 79 | 2 | 0 |
| | S1 | 3 | 79 | M | 181 | 79 | 5 | 1 |
| | S1 | 4 | 79 | M | 181 | 79 | 3 | 1 |
| | S1 | 5 | 79 | M | 181 | 79 | 0 | 0 |
| | S2 | 6 | 59 | M | 180 | 93 | 0 | 0 |
| | S2 | 7 | 59 | M | 180 | 93 | 0 | 0 |
| | S2 | 8 | 59 | M | 180 | 93 | 0 | 0 |
| | S2 | 9 | 59 | M | 180 | 93 | 0 | 0 |
| | S3 | 10 | 74 | M | 173 | 47 | 1 | 0 |
| | S3 | 11 | 74 | M | 173 | 47 | 1 | 0 |
| | S3 | 12 | 74 | M | 173 | 47 | 2 | 0 |
| | S3 | 13 | 74 | M | 173 | 47 | 3 | 1 |
| | T0503 | 1 | 79 | M | 180 | 65.8 | 0 | 0 |

| | | | | | | | | |
|---|---|---|---|---|---|---|---|---|
| Shaw 2006 [8] | T0503 | 2 | 79 | M | 180 | 65.8 | 0 | 0 |
| | T0504 | 3 | 80 | M | 165 | 80.7 | 0 | 0 |
| | T0504 | 4 | 80 | M | 165 | 80.7 | 0 | 0 |
| | T0505 | 5 | 77 | M | 178 | 66.2 | 1 | 0 |
| | T0505 | 6 | 77 | M | 178 | 66.2 | 4 | 1 |
| | T0506 | 7 | 87 | M | 175 | 65.7 | 1 | 0 |
| | T0506 | 8 | 87 | M | 175 | 65.7 | 2 | 0 |
| | T0507 | 9 | 53 | M | 165 | 65.3 | 0 | 0 |
| | T0507 | 10 | 53 | M | 165 | 65.3 | 1 | 0 |
| | T0601 | 11 | 63 | M | 186 | 93 | 0 | 0 |
| | T0601 | 12 | 63 | M | 186 | 93 | 0 | 0 |
| | T0602 | 13 | 79 | M | 164 | 74.8 | 0 | 0 |
| | T0602 | 14 | 79 | M | 164 | 74.8 | 0 | 0 |
| Robbins 1979 [9] | 76T062 | 1 | 69 | M | 174.3 | 50.1 | 7 | 1 |
| | 76T065 | 2 | 63 | M | 178.9 | 94.7 | 0 | 0 |
| | 77T071 | 3 | 60 | M | 172.2 | 80.7 | 0 | 0 |
| | 77T074 | 4 | 60 | M | 176.9 | 54 | 2 | 0 |
| | 77T077 | 5 | 79 | M | 175.5 | 73.7 | 3 | 1 |
| | 77T080 | 6 | 64 | M | 170.2 | 40.8 | 16 | 1 |
| Trosseille 2008 [10] | 586 | 1 | 74 | M | 176 | 77 | 4 | 1 |
| | 587 | 2 | 82 | M | 180 | 78 | 12 | 1 |
| Leport 2011 [11] | 606 | 1 | 87 | M | 171 | 71 | 18 | 1 |
| | 613 | 2 | 65 | F | 160 | 73 | 7 | 1 |
| | 614 | 3 | 80 | M | 178 | 56.5 | 18 | 1 |
| | 620 | 4 | 79 | M | 167 | 63.5 | 21 | 1 |
| | 605 | 5 | 73 | M | 171 | 61 | 4 | 1 |
| | 612 | 6 | 82 | M | 162 | 62 | 14 | 1 |
| | 616 | 7 | 55 | M | 175 | 63 | 9 | 1 |
| | 619 | 8 | 83 | M | 170 | 73.5 | 19 | 1 |
| Kemper 2008 [12] | 1 | Tside1_2 | 61 | M | 167 | 69.1 | 0 | 0 |
| | 2 | Tside2_2 | 47 | M | 170 | 64.3 | 0 | 0 |
| | 3 | Tside3_4 | 56 | M | 165 | 63.2 | 0 | 0 |
| | 4 | Tside4_4 | 49 | M | 170 | 71.8 | 0 | 0 |
| Chung 1999 [13] | CAD1 | 1 | 54 | M | N/A | 103 | 4 | 1 |
| | CAD4 | 2 | 71 | M | N/A | 76 | 15 | 1 |
| | CAD5 | 3 | 79 | F | N/A | 71 | 11 | 1 |
| | CAD6 | 4 | 45 | M | N/A | 82 | 10 | 1 |
| | CAD2 | 5 | 52 | M | N/A | 84 | 17 | 1 |
| | CAD3 | 6 | 60 | F | N/A | 65 | 15 | 1 |
| Compigne 2004 [14] | SIBER01 | LCC01 | 77 | F | 161 | 67 | 6 | 1 |
| | SIBER02 | LCC03 | 88 | M | 163 | 33 | 18 | 1 |
| | SIBER03 | LCC05 | 79 | F | 159 | 52 | 17 | 1 |
| | SIBER04 | LCC07 | 82 | F | 155 | 50 | 14 | 1 |
| | SIBER06 | LCC10 | 94 | F | 148 | 50 | 12 | 1 |
| Petit 2019 [15] | 736 | FARSIDE3 | 74 | M | 181 | 86 | 3 | 1 |
| | 737 | FARSIDE4 | 82 | M | 161 | 64 | 8 | 1 |
| | 738 | FARSIDE5 | 88 | M | 169 | 63 | 0 | 0 |
| | 739 | FARSIDE9 | 73 | M | 173 | 62 | 3 | 1 |
| | 740 | FARSIDE10 | 87 | M | 172 | 72 | 6 | 1 |

| | | | | | | | | |
|---|---|---|---|---|---|---|---|---|
| | 741 | FARSIDE11 | 91 | M | 176 | 66 | 1 | 0 |
| Lessley 2010 [16] | 468 | 1413 | 67 | M | 166 | 59.9 | 16 | 1 |
| | 473 | 1414 | 54 | M | 182 | 63.1 | 0 | 0 |
| | 480 | 1415 | 71 | M | 182 | 68.9 | 0 | 0 |
| Shaw 2014 [19] | -- | 1569 | 69 | M | 168 | 93.4 | 0 | 0 |
| | -- | 1570 | 49 | M | 175 | 98.0 | 2 | 0 |
| | -- | 1571 | 70 | M | 165 | 67.6 | 9 | 1 |
| Maltese 2002 [20] | -- | 3324 | 77 | M | N/A | 75 | 3 | 1 |
| | -- | 3325 | 63 | M | N/A | 61 | 22 | 1 |
| | -- | 3422 | 44 | M | N/A | 83 | 16 | 1 |
| | -- | 3423 | 49 | M | N/A | 62 | 3 | 1 |
| | -- | 3577 | 74 | F | N/A | 52 | 5 | 1 |
| | -- | 3578 | 73 | F | N/A | 51 | 24 | 1 |
| | -- | 3579 | 68 | M | N/A | 98 | 16 | 1 |
| | -- | 3585 | 72 | M | N/A | 73 | 8 | 1 |
| | -- | 3587 | 63 | M | N/A | 100 | 17 | 1 |
| | -- | 3589 | 67 | M | N/A | 76 | 12 | 1 |
| | -- | 4218 | 68 | M | N/A | 81 | 7 | 1 |
| | -- | 4268 | 54 | M | N/A | 90 | 7 | 1 |
| | -- | 4295 | 51 | F | N/A | 52 | 5 | 1 |
| | -- | 3120 | 73 | M | N/A | 89 | 6 | 1 |
| | -- | 3122 | 27 | M | N/A | 72 | 7 | 1 |
| | -- | 3155 | 55 | M | N/A | 76 | 0 | 0 |
| | -- | 3588 | 72 | M | N/A | 66 | 7 | 1 |
| | -- | 3663 | 75 | F | N/A | 42 | 8 | 1 |
| | -- | 3664 | 67 | F | N/A | 74 | 8 | 1 |
| | -- | 3700 | 86 | M | N/A | 67 | 0 | 0 |
| | -- | 3535 | 78 | M | N/A | 88 | 6 | 1 |
| | -- | 3536 | 84 | M | N/A | 76 | 8 | 1 |
| | -- | 3537 | 79 | M | N/A | 93 | 8 | 1 |
| | -- | 4296 | 39 | M | N/A | 66 | 10 | 1 |
| | -- | 4338 | 46 | F | N/A | 69 | 7 | 1 |
| Cavanaugh 1993 [21] | -- | 1 | 60 | M | 176 | 70.5 | 31 | 1 |
| | -- | 2 | 64 | F | 163 | 49.5 | 35 | 1 |
| | -- | 3 | 37 | M | 175 | 70.0 | 24 | 1 |
| | -- | 4 | 69 | M | 163 | 57.6 | 22 | 1 |
| | -- | 5 | 67 | M | 172 | 44.0 | 20 | 1 |
| | -- | 6 | 60 | M | 182 | 61.2 | 13 | 1 |
| | -- | 7 | 66 | M | 170 | 74.8 | 16 | 1 |
| | -- | 8 | 64 | F | 162 | 73.9 | 24 | 1 |
| | -- | 9 | 61 | F | 165 | 54.9 | 34 | 1 |
| | -- | 10 | 60 | M | 171 | 62.1 | 5 | 1 |
| | -- | 11 | 54 | F | 165 | 55.3 | 3 | 1 |
| | -- | 12 | 68 | F | 143 | 54.4 | 25 | 1 |
| | -- | 13 | 62 | M | 161 | 66.7 | 18 | 1 |
| | -- | 14 | 60 | M | 174 | 55.3 | 18 | 1 |
| | -- | 15 | 43 | F | 154 | 68.9 | 0 | 0 |
| | -- | 16 | 58 | F | 170 | 56.7 | 26 | 1 |
| | -- | 17 | 65 | M | 170 | 93.0 | 2 | 0 |

***Table A2: Impactor Masses and Velocities for Impactor Cases***

| Ref. | PMHS_ID | Test_ID | Test Impactor Mass (kg) | Test Impactor Initial Velocity (m/s) | Scaled impactor mass for THUMS v4.1 (kg) |
|---|---|---|---|---|---|
| Viano 1989 [6] – Chest | 863 | 2 | 23.4 | 9.4 | 16.4303 |
| | RNY1 | 3 | 23.4 | 8.7 | 39.9555 |
| | 935 | 4 | 23.4 | 5.99 | 25.1688 |
| | 947 | 5 | 23.4 | 6.48 | 31.2541 |
| | 954 | 7 | 23.4 | 6.73 | 31.2541 |
| | RNY2 | 9 | 23.4 | 6.71 | 28.498 |
| | 956 | 11 | 23.4 | 6.71 | 23.0714 |
| | 993 | 14 | 23.4 | 8.3 | 24.8451 |
| | 986 | 17 | 23.4 | 5.5 | 25.0077 |
| | 986 | 18 | 23.4 | 9.7 | 25.0077 |
| | 8 | 29 | 23.4 | 5.2 | 33.1269 |
| | 8 | 33 | 23.4 | 9.7 | 33.1269 |
| | U0M1 | 36 | 23.4 | 4 | 26.0104 |
| | U0M1 | 37 | 23.4 | 10.2 | 26.0104 |
| | U0M2 | 40 | 23.4 | 3.62 | 23.2054 |
| | U0M2 | 41 | 23.4 | 3.8 | 23.2054 |
| Viano 1989 [6] – Abdomen | 947 | 6 | 23.4 | 6.79 | 31.25408 |
| | 954 | 8 | 23.4 | 6.73 | 31.25408 |
| | RNY2 | 10 | 23.4 | 6.75 | 28.49801 |
| | 956 | 12 | 23.4 | 7.08 | 23.07142 |
| | 993 | 15 | 23.4 | 8.1 | 24.84514 |
| | 986 | 19 | 23.4 | 5.1 | 25.00771 |
| | 986 | 20 | 23.4 | 9.8 | 25.00771 |
| | 47 | 23 | 23.4 | 5.5 | 20.95152 |
| | 47 | 24 | 23.4 | 5.4 | 20.95152 |
| | 47 | 28 | 23.4 | 9.9 | 20.95152 |
| | 8 | 30 | 23.4 | 5.1 | 33.12685 |
| | 63 | 34 | 23.4 | 9.8 | 36.21842 |
| | U0M2 | 42 | 23.4 | 3.82 | 23.20541 |
| | U0M2 | 43 | 23.4 | 3.8 | 23.20541 |
| Subit 2010 [7] | S1 | 1 | 71.8 | 1 | 68.2827 |
| | S1 | 2 | 71.8 | 3 | 68.2827 |
| | S1 | 3 | 71.8 | 6 | 68.2827 |
| | S1 | 4 | 71.8 | 1 | 68.2827 |
| | S1 | 5 | 71.8 | 3 | 68.2827 |
| | S2 | 6 | 71.8 | 3 | 58.0036 |
| | S2 | 7 | 71.8 | 3 | 58.0036 |
| | S2 | 8 | 71.8 | 3 | 58.0036 |
| | S2 | 9 | 71.8 | 3 | 58.0036 |
| | S3 | 10 | 71.8 | 3 | 114.773 |
| | S3 | 11 | 71.8 | 3 | 114.773 |
| | S3 | 12 | 71.8 | 3 | 114.773 |

| | | | | | |
|---|---|---|---|---|---|
| | S3 | 13 | 71.8 | 3 | 114.773 |
| Shaw 2006 [8] | T0503 | 1 | 23.4 | 2.51 | 26.718 |
| | T0503 | 2 | 23.4 | 2.58 | 26.718 |
| | T0504 | 3 | 23.4 | 2.43 | 21.7849 |
| | T0504 | 4 | 23.4 | 2.61 | 21.7849 |
| | T0505 | 5 | 23.4 | 2.45 | 26.5565 |
| | T0505 | 6 | 23.4 | 2.47 | 26.5565 |
| | T0506 | 7 | 23.4 | 2.55 | 26.7586 |
| | T0506 | 8 | 23.4 | 2.54 | 26.7586 |
| | T0507 | 9 | 23.4 | 2.48 | 26.9225 |
| | T0507 | 10 | 23.4 | 2.57 | 26.9225 |
| | T0601 | 11 | 23.4 | 2.57 | 18.9037 |
| | T0601 | 12 | 23.4 | 2.48 | 18.9037 |
| | T0602 | 13 | 23.4 | 2.48 | 23.5032 |
| | T0602 | 14 | 23.4 | 2.44 | 23.5032 |
| Robbins 1979 [9] | 76T062 | 1 | 23.4 | 6.08 | 35.09066 |
| | 76T065 | 2 | 23.4 | 6.08 | 18.56433 |
| | 77T071 | 3 | 23.4 | 6.08 | 21.78491 |
| | 77T074 | 4 | 23.4 | 6.08 | 32.55633 |
| | 77T077 | 5 | 23.4 | 4.25 | 23.85403 |
| | 77T080 | 6 | 23.4 | 4.25 | 43.08926 |
| Trosseille 2008 [10] | 586 | 1 | 23.4 | 4.4 | 22.83171 |
| | 587 | 2 | 23.4 | 4.2 | 22.539 |
| Leport 2011 [11] | 606 | 1 | 23.4 | 4.2 | 24.76115 |
| | 613 | 2 | 23.4 | 4.2 | 24.08277 |
| | 614 | 3 | 23.4 | 6.5 | 31.11579 |
| | 620 | 4 | 23.4 | 6.5 | 27.6857 |
| | 605 | 5 | 23.4 | 4.3 | 28.82036 |
| | 612 | 6 | 23.4 | 4.3 | 28.35552 |
| | 616 | 7 | 23.4 | 6.5 | 27.90543 |
| | 619 | 8 | 23.4 | 6.5 | 23.91894 |
| Kemper 2008 [12] | 1 | Tside1_2 | 16 | 3 | 17.39624 |
| | 2 | Tside2_2 | 16 | 3 | 18.69487 |
| | 3 | Tside3_4 | 16 | 3 | 19.02025 |
| | 4 | Tside4_4 | 16 | 3 | 16.74206 |
| Chung 1999 [13] | CAD1 | 1 | 50 | 5.6 | 36.4709 |
| | CAD4 | 2 | 50 | 5.6 | 49.4276 |
| | CAD5 | 3 | 50 | 5.6 | 52.9085 |
| | CAD6 | 4 | 50 | 5.6 | 45.811 |
| | CAD2 | 5 | 50 | 5.6 | 44.7202 |
| | CAD3 | 6 | 50 | 5.6 | 57.7923 |
| Compigne 2004 [14] | SIBER01 | LCC01 | 23.4 | 4.1 | 26.23943 |
| | SIBER02 | LCC03 | 23.4 | 4.2 | 53.274 |
| | SIBER03 | LCC05 | 23.4 | 4.2 | 33.8085 |
| | SIBER04 | LCC07 | 23.4 | 4.2 | 35.16084 |
| | SIBER06 | LCC10 | 23.4 | 4.2 | 35.16084 |